



IMAGE PROCESSING TECHNIQUE FOR SHEAR- STRESS OPTICAL MEASUREMENTS

Vladimir Fonov, Sergey Fonov, Grant Jones, Jim Crafton
Innovative Scientific Solutions Inc.

Keywords: *shear stress, S³F, image processing*

ABSTRACT

A new method for measuring surface pressure and shear force based on elastic polymers has been developed. This technique (Surface Stress Sensitive Film, S³F) requires extensive data processing, i.e., processing of image pairs into 3D surface deformations and the transformation of these deformations into applied surface forces.

This paper describes an analysis method used to determine the 2D lateral surface displacement of S³Fs. This hybrid method is based on cross-correlation and optical-flow techniques. Test results with synthetic images are reported in this paper.

Experimental results with the S³F technique using the new analysis algorithms have been obtained in both water and air environments. Results from a low-speed (10 - 15m/s) vortex-generator are presented.

1. BACKGROUND

In the past, two-dimensional distributions of shear stress were determined using liquid crystals [1] or oil film measurements [2]. In 1990, Tarasov and Fonov presented a new method for the direct measurement of surface shear forces [3,4]. Their method incorporated a sensing element on the model surface that included a film made of a flexible (elastic) polymer. The thickness and shear modulus of the polymer was controlled in an effort to produce a gauge with the appropriate sensitivity. Local tangential film deformations were determined by tracking the relative displacement of markers applied to the upper and lower film surfaces. Shear stress was determined using Hooke's law. The markers could take the form of a grating that was placed on the model surface under the film. The use of a transmitting grating on film surface enabled the use of a moiré fringe pattern to visualize the shear deformation field. This method provided improved accuracy and spatial resolution due to the image based detection technique for determining local values of the shear stress. The main issue with this method was the fact that a gradient in the normal pressure also creates a shear displacement, therefore, the method worked best only in the absence of normal pressure gradients.

2. S³F TECHNIQUE

The standard approach for resolving small increments in pressure is to increase the sensitivity of the gauge and measure only the difference in pressure. The concept of a differential pressure measurement is the cornerstone of the S³F method. Take for example two discrete pressure loads applied to the surface of the elastic polymeric film. The film behaves like a non-compressible fluid, therefore, the change in the local layer thickness is a function of the difference between the two applied pressures. Contrary to standard fluids, the film is an elastic media and therefore endeavors to recover its original shape upon removal of the load.

More details on the physical basics of the S³F method are discussed by Fonov, et al., [5]. This paper focuses on the data registration and processing techniques used to determine 2D lateral displacements of the elastic polymeric film.

3. EXPERIMENTAL ARRANGEMENT

0 shows the experimental set-up for measuring shear and stress forces using the S^3F approach. A typical setup consists of the model under study, covered with S^3F , illumination system, and imaging system (scientific-grade CCD camera). The 3D deformation of the S^3F is observed by using randomly distributed particles (embedded into S^3F 's surface) and measuring the change in film thickness.

3.1. Data Processing Outline

1. Images of the model in wind-on and wind-off conditions are taken, with optimally dark images and flat field images (see 0).
2. Image processing software (discussed in this paper) is used to extract 2D displacement vectors and relative film thickness (see 0).
3. Deformation fields obtained from the previous steps are mapped onto 3D model grid.
4. Transformation from film deformation into surface shear stress and normal pressure forces is accomplished (discussed by Fonov, et al., [5]).

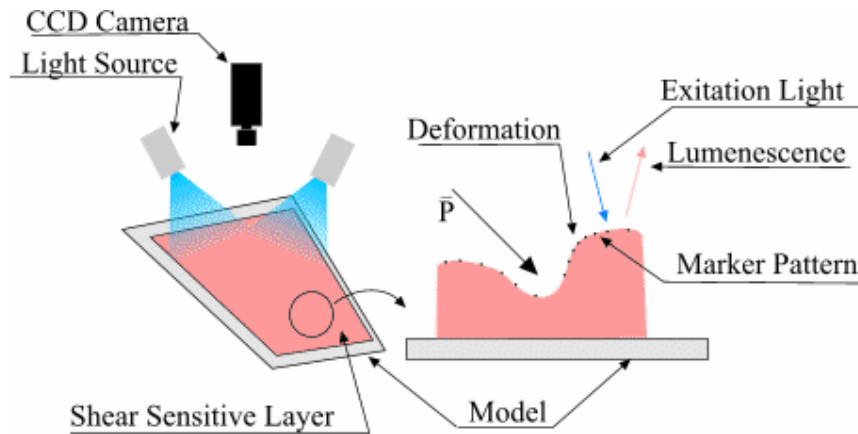


Fig. 1 - Local surface stress estimated by observing deformations of thin film.

4. IMAGE PROCESSING ALGORITHM

4.1. Estimation of the local deformations

Algorithms for estimating the deformation image pairs are widely used in many fields, including Particle Image Velocimetry, Machine Vision etc. An extensive review of the different techniques is given by Brown [6]. S^3F measurements require high precision to evaluate the displacement vectors with reasonable robustness against noise--similar to PIV particle images with high seed densities. The techniques developed by XXX. [X] for the image alignment in PSP experiments was adopted for use with the S^3F technique. This algorithm is a hybrid, using phase correlation [7] to estimate integer (in pixels) part of the displacement vector and an optical-flow based method to estimate the sub-pixel part of the displacement.

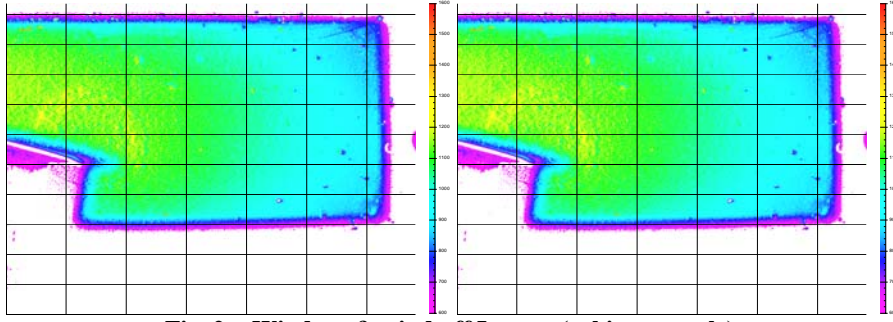


Fig. 2. - Wind-on & wind-off Images (arbitrary scale).

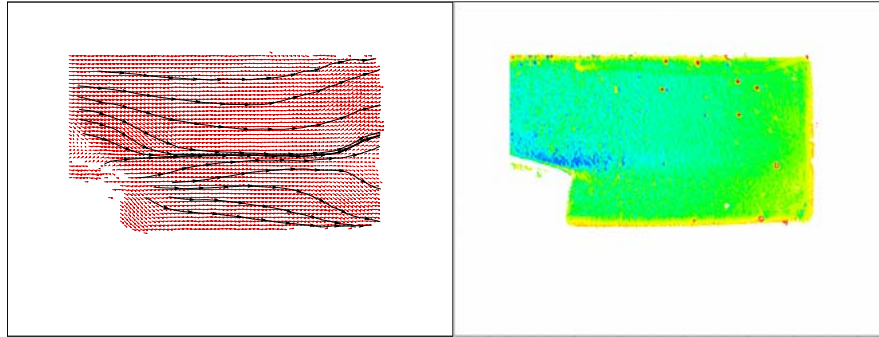


Fig 3. - Displacement vectors and intensity ratio (arbitrary scale).

4.2. Phase-correlation image registration

This method is based on the properties of the Fourier transform applied to two images that are shifted relative to each other. The Fourier transform of an image $f(x,y)$ is a complex function which can be expressed in exponential form:

$$F(\omega_x, \omega_y) = |F(\omega_x, \omega_y)| e^{i\phi(\omega_x, \omega_y)} \quad (1)$$

where $|F(\omega_x, \omega_y)|$ is the magnitude of the Fourier transform and $\phi(\omega_x, \omega_y)$ is the phase angle.

Phase correlation relies on the translation property of the Fourier transform sometimes referred to as the Shift Theorem. Given two images f_1 and f_2 which differ only by a displacement (d_x, d_y) , i.e $f_2(x, y) = f_1(x - d_x, y - d_y)$, their corresponding Fourier transforms F_1 and F_2 will be related by Eq. (2)

$$F_2(\omega_x, \omega_y) = e^{-i(\omega_x d_x + \omega_y d_y)} F_1(\omega_x, \omega_y) \quad (2)$$

If the cross-power spectrum of the two images (3) is computed, the Shift Theorem guarantees that the phase of the cross-power spectrum is equivalent to the phase difference between the images.

$$\frac{F_1(\omega_x, \omega_y) F_2^*(\omega_x, \omega_y)}{|F_1(\omega_x, \omega_y) F_2^*(\omega_x, \omega_y)|} = e^{i(\omega_x d_x + \omega_y d_y)} \quad (3)$$

By taking the inverse Fourier transform of the cross-power spectrum the displacement will be represented by an impulse at the corresponding coordinates. Since the phase difference for every frequency contributes equally, the location of the peak will not be strongly affected by narrow-bandwidth noise, which may be the case for conventional cross-correlations.

Several authors [8,11] have studied similar methods in the evaluation of sub-pixel displacements. Particularly, Sjudahl [8] analysed the effects of noise and rotation on the accuracy

of determining displacements in speckle photography. In general, it is possible to obtain a subpixel estimation of the displacement by calculating the centroid of the cross-correlation or phase-correlation peak.

For our algorithm, a different approach was used for estimating the sub-pixel displacement. It was found that the following method provided better stability against noise for S³F applications (a similar algorithm was proposed by Cheng-Yuan, et al., [7])

4.3. Optical Flow & Phase Correlation

- In the first stage, the displacement is estimated with either a phase or cross-correlation algorithm, with a precision of 1 pixel.
- In the second stage, the residual displacement is evaluated using a method similar to the optical flow calculation of Cheng-Yuan, et al., [8].

$$I_2(x, y) = I_1(x + d_x, y + d_y) = I_1(x, y) + gradI_1(x, y) \cdot (d_x, d_y) \quad (4)$$

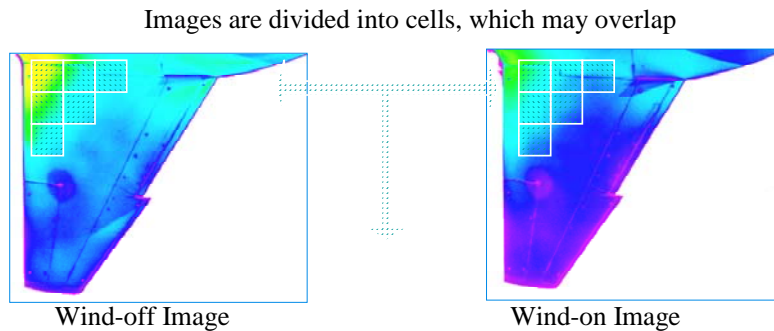
- The sub-pixel displacement is then found using a least-square approximation:

$$(d_x, d_y) = \arg \min_{(d_x, d_y)} \left(I_2(x, y) - I_1(x, y) - gradI_1(x, y) \cdot (d_x, d_y) \right)^2 \quad (5)$$

- For computations, the gradient $gradI_1(x, y)$ is evaluated using a convolution of the original image I_1 with Gaussian gradient filters (one for each direction) [13]. By varying the parameter σ of the Gaussian kernel, it is possible to vary the sensitivity of the method to noise.

4.4. Data Processing Algorithm

In the actual data-processing (0) images in wind-off and wind-on condition are divided into areas of interrogation (cells). For each pair of cells phase-correlation and optical flow algorithm is applied, producing one 2D vector. Resulting vector field may-be filtered and interpolated.



For each cell cross-correlation or phase-correlation and optical flow calculated, and displacement vector estimated.

Fig 4. - Data processing flow.

The sensitivity to the local variations in the displacement field depends on the size of the cell, and the distance between their centers. Unfortunately, the maximum displacement is limited by the size of cell. Sometimes, to achieve the required sensitivity and magnitude of the displacements, it is necessary to implement this technique in several hierarchical iterations (0)

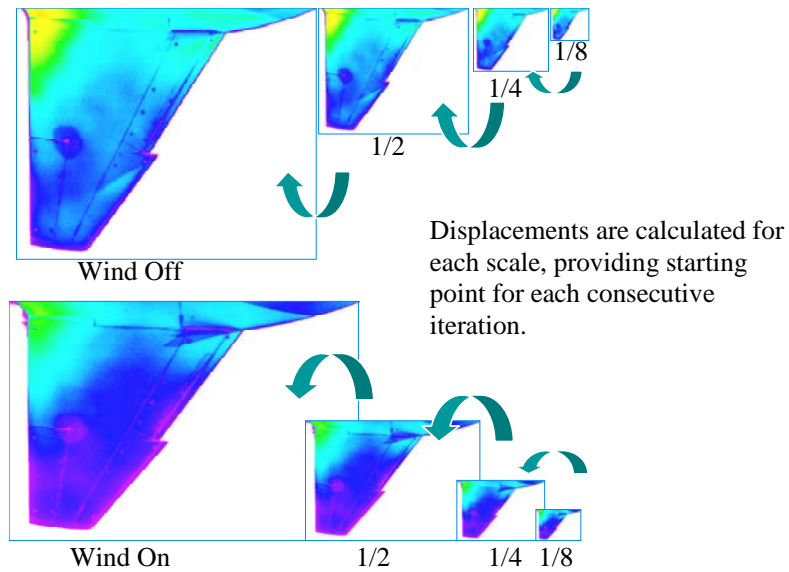


Fig 5. - Hierarchical calculations of the displacement vectors

4.5. Testing

The new algorithm was tested on images obtained with a production imaging system, using synthetic random patterns (0), under linear and rotation translations (0). Images were processed with the hybrid (Phase Correlation + Optical Flow) algorithm and the Phase-Correlation (only) based algorithm. The results of this comparison shown in Figs. 8-10, demonstrated a significant improvement in the accuracy for some cases.

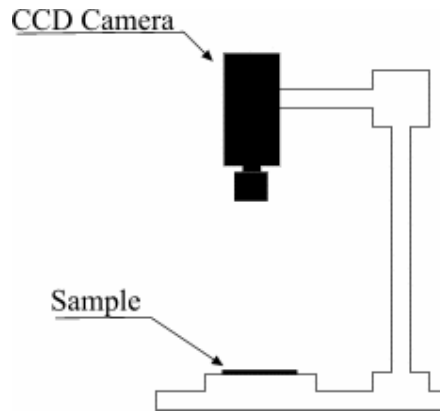


Fig. 6 - Test setup.

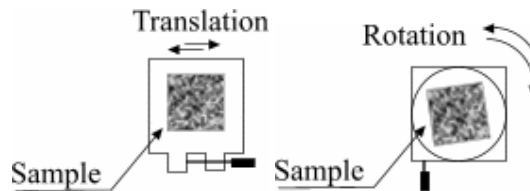


Fig. 7 - Test cases.

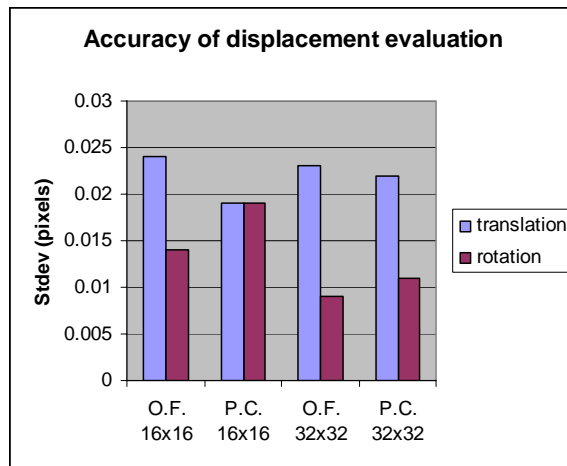


Fig. 8 - Standard deviation of displacement evaluation for hybrid algorithm (O.F.) and Phase Correlation centroid algorithm (P.C.) showed for cells 16x16 pixels and 32x32 pixels.

It is worth mentioning that in some cases the phase-correlation (only) based algorithm showed less deviation in the results than the hybrid algorithm. This is probably due to its deviation being less dependant on the magnitude of the displacement. In 0-10 there are visible areas close to the center of rotation (zero distance) where the deviation of the hybrid algorithm has much less magnitude in comparison with the almost constant deviation of the phase-correlation (only) based algorithm.

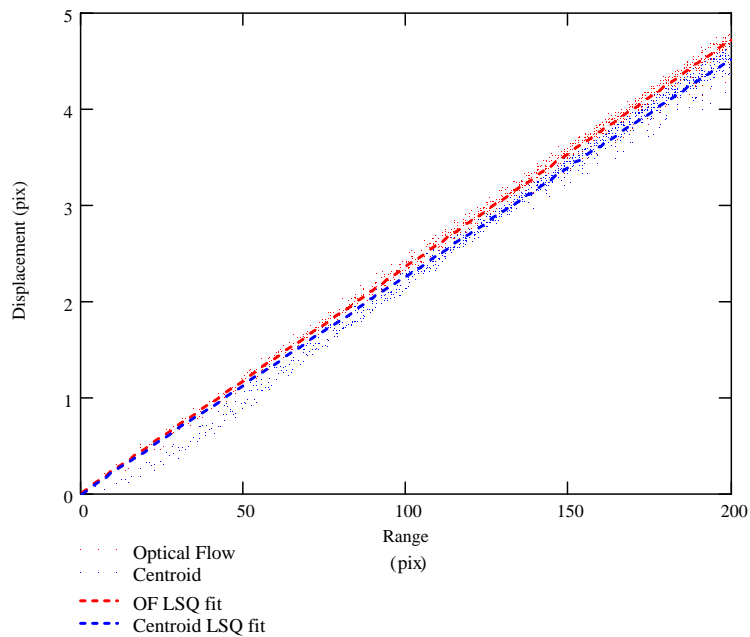


Fig 9. - Tangential translation estimation (rotation case), cellsize 16x16 pixels, 50% overlapping.

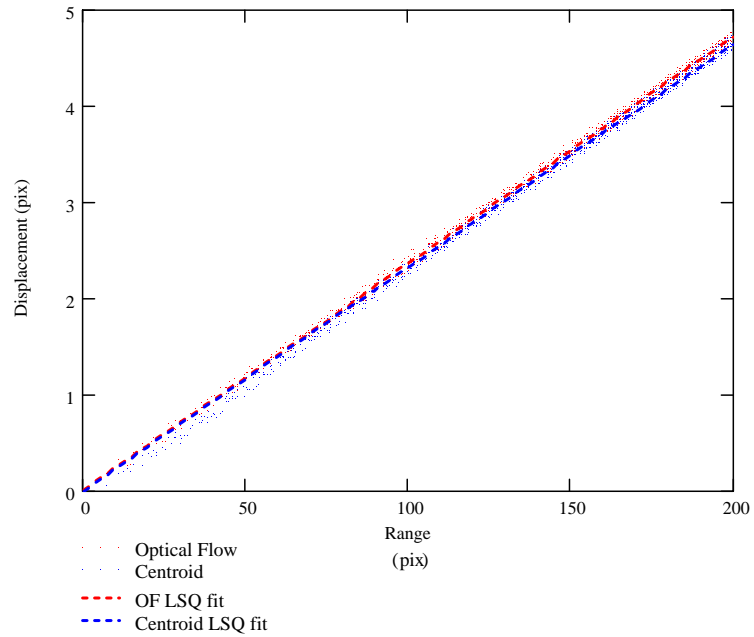


Fig. 10 - Tangential translation estimation (rotation case), cell size 32x32 pixels, 75% overlapping.

5. VORTEX GENERATOR EXPERIMENT

As a demonstration of the S³F method, an experiment was performed in the ISSI low speed wind tunnel. 0 outlines the setup used to demonstrate the applicability of the S³F method in low speed flows.

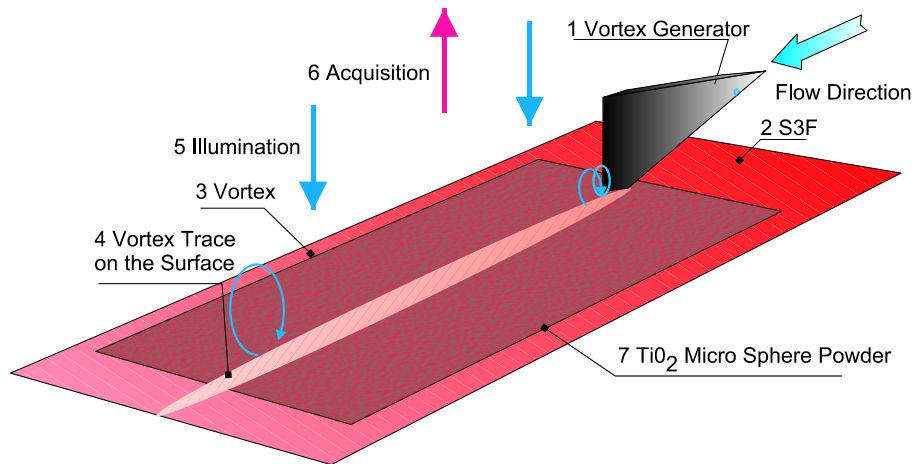


Fig. 11 - Schematic experimental set-up, velocity of the flow 15 m/s.

This experiment resulted in the two-dimensional displacement field (0) and the film thickness field (0).

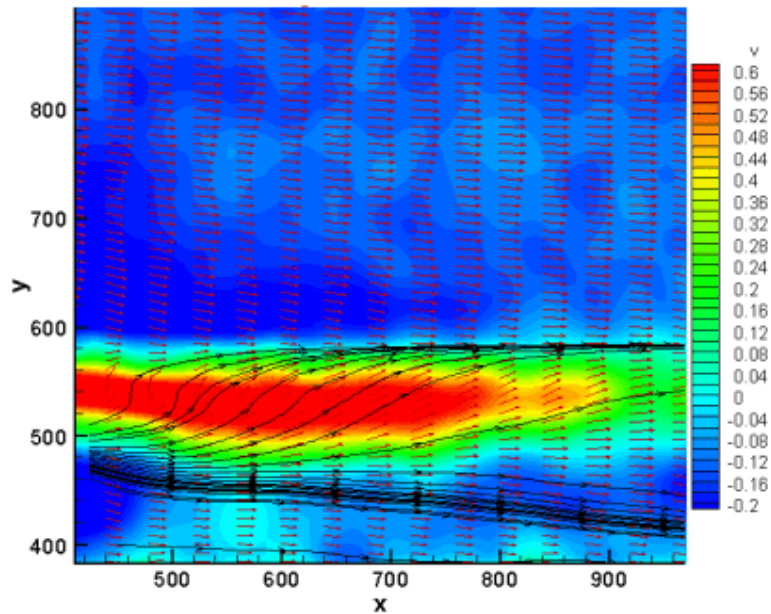


Fig. 12 - Experimental results obtained in the low-speed wind tunnel. Color component denotes vertical component of the displacement field (in pixels).

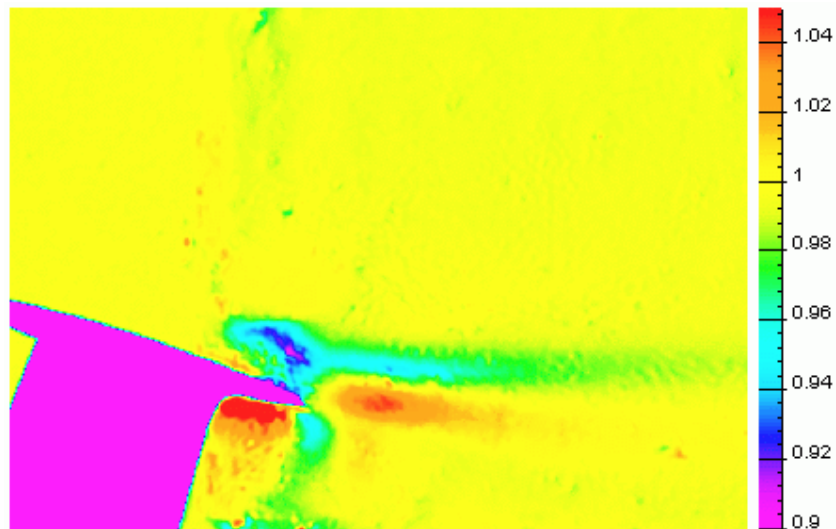


Fig. 13 - Experimental results obtained in low-speed wind tunnel. Relative thickness of the S^3F .

6. CONCLUSIONS

This paper reports the development of a novel hybrid algorithm for determining the 2D lateral displacement of S^3F layers. The hybrid phase-correlation and optical flow algorithm displayed a significant improvement in the subpixel accuracy of displacement peaks. This new algorithm helps to ensure the accuracy required in transforming the S^3F layer deformation into the applied surface loads.

7. FUTURE RESEARCH

Following areas require additional work for the S^3F technique:

- Resection of the 2D displacement and film thickness fields into the 3D model geometry.
- The calibration procedure and transformation from film deformation into pressure fields.
- Automatic compensation for model displacement and deformation.

REFERENCES

1. Reda D.V. "Measurements of continuous pressure and shear distributions using coating and imaging techniques", AIAA Journal v.36, pp. 895-899, 1998
2. Zhong, S. "Detection of flow separation and reattachment using shear-sensitive liquid crystals", Experiment in Fluids, v.32 pp.667-673, 2002
3. Tarasov V.N, Orlov A.A. "Method for determining shear stress on aerodynamic model surface", Patent of Russia, 4841553/23/1990
4. Tarasov V., S. Fonov, A. Morozov, "New gauges for direct skin friction measurements." Proc. Of 17th International Congress on Instrumentation in Aerospace Simulation Facilities (ICIASF), Monterey, California, 29 Sept to 2 Oct 1997.
5. Fonov S. D. et al. 2004 NEW METHOD FOR SURFACE PRESSURE MEASUREMENTS. To be presented in Flow-Visualization Conference, University of Notre Dame, Indiana, USA 2004.
6. Brown L. G. 1992 "A Survey of Image Registration Techniques" ACM Computing Surveys, Vol 24, No. 4, December 1992
7. Cheng-Yuan Tang, Yi-Ping Hung, and Zen Chen. "Robust two-stage approach for image motion estimation", Electronics Letters, Vol. 34, No. 11, pp. 1091-1093, May 1998.
8. Sjudahl M. 1994 Electronic speckle photography: increased accuracy by nonintegral pixel shifting. Applied Optics, 1 October 1994, Vol. 33, No. 28
9. Barron J. L., Fleet D. J., Beauchemin S. S., and Burkitt T. A.. Performance of optical flow techniques. IEEE Computer Society Conference on Computer Vision and Pattern Recognition, 1992
10. Fonov V.S. Development and Analysis of Data Processing Methods Applied to Luminescent Coating Systems in Aerodynamics. PhD thesis Heriot-Watt University 2002.
11. Shekarforoush H., Berthod M., and Zerubia J. 1996 Subpixel image registration by estimating the polyphase decomposition of cross power spectrum. In Computer vision and pattern recognition, pp. 532-537, Los Alamitos, CA, 1996. IEEE computer society press.
12. Black M. J. Anadan P. A. 1993 Framework for the robust estimation of Optical Flow. Presented at 4th international conference on computer vision 1993 (ICCV93)
13. Olsen O. F. 1996 Multi-Scale Segmentation of Grey-Scale Images. Technical Report DIK U-96-30 August 1996